2013 Conference on Control and Fault-Tolerant Systems (SysTol)
October 9-11, 2013. Nice, France

Optimised Sensor Selection for Control: A Hardware-in-the-Loop Realization on FPGA for an EMS System

Kyriakos M. Deliparaschos[1*], Konstantinos Michail[2], Spyros G. Tzafestas[3] and Argyrios C. Zolotas[4]

Abstract— **This paper presents a Hardware-in-the-loop (HIL) approach on a Field Programmable Gate Array (denoted as FPGA-in-the-loop and abbreviated as FIL) for the optimised sensor selection task of controlling a MAGnetic LEVitation (MAGLEV) system. A recently proposed systematic framework for optimised sensor selection for control and fault tolerance is developed in [1]. The framework was validated using realistic simulations on an electromagnetic suspension system. In this work, the sensor selection framework for control, and practical validation of the controller on FPGA (via HIL concept) applied on an electromagnetic suspension are considered.**

I. INTRODUCTION

The task of sensor set selection in an optimised manner for control design is a non-trivial task to do; especially if there is a large number of sensor candidates to select from. A typical high integrity system requires both control and reliable operation. Optimised performance, robustness, fault tolerance, and low complexity are the main goals of the designer. In [1], a systematic framework for control and fault tolerance is proposed, which takes into account the aforementioned requirements for a MAGLEV suspension system at simulation level. The framework combines Linear Quadratic Gaussian (LQG) control [2], multiobjective optimisation with Genetic Algorithms (GAs) [3], and reconfigurable fault tolerant control methods [4]. The electromagnetic suspension system was used to test the efficacy of the proposed framework and the outcome results have shown a high potential for industrial applications.

In this paper the authors are using the Hardware-in-the-loop concept (HIL) [5] to practically integrate the controllers on the FPGA chip [6], while the model under control is implemented in a high-level simulation environment (MATLAB/Simulink). The HIL technique is a method widely known that is used in the development and test of complex real-time control systems by effectively adding the complexity of the plant under control to the test platform [7], [8]. The model of the system is realised in a soft form and usually modelled using a high-level language (e.g., MATLAB) or a graphical model-based design tool (e.g., Simulink). The HIL idea is illustrated in Fig. 1. The overall diagram depicts the model of the plant (implemented on a software-based code) that interfaces with the actual controller (realised on an FPGA) via a communication link. The HIL is realised on Xilinx Spartan-6 Family SP605 FPGA board [9]. The advantage of using FPGAs to process large test data sets allows to rapidly evaluate algorithms and test designs under real-world scenarios avoiding heavy time penalty associated with Hardware Description Language (HDL) simulators. For the prototyping of the proposed approach, a fusion of system modelling, verification and Electronic Design Automation (EDA) tools such MATLAB/Simulink, Xilinx ISE, and Mentor Modelsim were used.

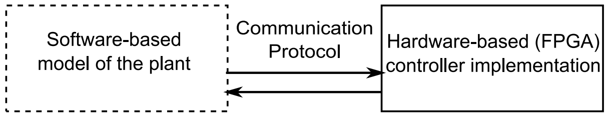

Fig. 1. A simplified diagram of the Hardware-in-the-loop concept.

The contribution of this paper lies in the fact that the authors have obtained a practical implementation of LQG controllers, using the minimum number of sensors required to control the MAGLEV suspension system, subject to a set of non-trivial control requirements. The LQG controller is designed according to the separation principle, i.e., first a Linear Quadratic Regulator (LQR) is designed based on state feedback control theory, and then a Kalman-Bucy Estimator (KBE) is added in the loop, which estimates the states with various sensor sets. In the present work only the KBE is implemented in FIL.

The remainder of this paper is organised as follows. Section II outlines the modelling aspects of the maglev suspension system. Section III describes the systematic framework for optimised sensor selection with the FIL concept. Section IV introduces the KBE architecture and implementation on the FPGA, followed by Section V which presents the results from the practical KBE implementation with FIL as applied on the suspension. Section VI concludes with future directions of work.

II. THE CASE STUDY: MAGLEV SUSPENSION

A. Modelling

The single-stage electromagnetic suspension (EMS) that represents one quarter of a typical MAGLEV vehicle, is based on a typical U-core shape electromagnet. Details on the particular modelling exercise, can be found in [11]. The

[1*] Corresponding author. Department of Electrical and Computer Engineering and Informatics, Cyprus University of Technology, Limassol, Cyprus. k.deliparaschos@cut.ac.cy

[2] Department of Mechanical and Materials Science and Engineering, Cyprus University of Technology,Limassol,Cyprus. kon_michael@ieee.org

[3] School of Electrical and Computer Engineering, National Technical University of Athens, Greece. tzafesta@softlab.ntua.gr

[4] School of Engineering and Informatics, University of Sussex, United Kingdom. a.zolotas@sussex.ac.uk

978-1-4799-2854-5/13/$31.00 ©2013 European Union

non-linear model of the suspension can be expressed as,

$$\frac{dI}{dt} = \frac{V_c - IR_c + \frac{N_c A_p K_b}{G^2}\left(\frac{dz_t}{dt} - \frac{dZ}{dt}\right)}{\frac{N_c A_p K_b}{G} + L_c} \tag{1}$$

$$\frac{d^2 Z}{d^2 t} = g - \frac{K_f}{M_s}\frac{I^2}{G^2}, \qquad F = K_f B^2 \tag{2}$$

$$\frac{dG}{dt} = \frac{dz_t}{dt} - \frac{dZ}{dt}, \qquad B = K_b \frac{I}{G} \tag{3}$$

where V_c is the coil's voltage, F is the vertical force, I is the coil's current, G is the airgap, Z is the electromagnet's position, B is the flux density, M_s is the vehicle's mass, R_c is the coil's resistance, N_c is the number of turns, A_p is the pole face area and z_t is the track's position. Constants K_b, K_f and g are the flux, force and gravity constants with values equal to 0.0015, 0.0221 and $9.81m/s^2$ respectively. The linearisation of the non-linear model is based on small perturbations around the operating point, e.g., the airgap is assumed as $G = G_o + (z_t - z)$, where the lower case terms represent the small variation around the operating point, and subscript 'o' refers to the operating point. A similar approach is followed for B, F, I, V_c and Z (b,f,i,u_c and z respectively). The linearised state space description of the EMS is given by (4), with states $x = [i \quad \dot{z} \quad (z_t - z)]^T$, and an output equation that corresponds to the following five measurements: i, b, $(z_t - z)$, $\dot{z}$ and $\ddot{z}$. Assuming a total weight of $M_s = 1000kg$, the real world operating point values for the EMS system become: $G_o = 0.015m$, $B_o = 1T$, $I_o = 10A$, $V_o = 100V$ and $F_o = 9810N$. The parameters of the electromagnets, based on the operating point of the EMS, were calculated as: $R_c = 10\Omega$, $L_c = 0.1H$, $N_c = 2000$ and $A_p = 0.01m^2$.

$$\begin{aligned} \dot{x} &= Ax + B_{u_c} u_c + B_{\dot{z}_t} \dot{z}_t \\ y &= Cx \end{aligned} \tag{4}$$

where, A is the 3×3 state matrix, B_{u_c} is the 3×1 input matrix, $B_{\dot{z}_t}$ is the 3×1 disturbance matrix, and C is the $\alpha \times 3$ output matrix (α varies from 1 to 5, since its size changes according to the number of sensors in the sensor set). The aforementioned matrices are described by (5)-(8). The various sensor sets can be obtained by appropriate selection of the corresponding rows in the output matrix, C. The outputs of the MAGLEV are $y = [i, b, (z_t - z), \dot{z}, \ddot{z}]$.

$$A = \begin{bmatrix} -\frac{R_c}{L_c + \frac{K_b N_c A_p}{G_o}} & -\frac{K_b N_c A_p I_o}{G_o^2\left(L_c + \frac{K_b N_c A_p}{G_o}\right)} & 0 \\ -2K_f \frac{I_o}{M_s G_o^2} & 0 & 2K_f \frac{I_o^2}{M_s G_o^3} \\ 0 & -1 & 0 \end{bmatrix} \tag{5}$$

$$B_{u_c} = \begin{bmatrix} \frac{1}{L_c + \frac{K_b N_c A_p}{G_o}} & 0 & 0 \end{bmatrix}^T \tag{6}$$

$$B_{\dot{z}_t} = \begin{bmatrix} \frac{K_b N_c A_p I_o}{G_o^2\left(L_c + \frac{K_b N_c A_p}{G_o}\right)} & 0 & 1 \end{bmatrix}^T \tag{7}$$

$$C = \begin{bmatrix} 1 & 0 & 0 \\ \frac{K_b}{G_o} & 0 & -\frac{K_b I_o}{G_o^2} \\ 0 & 0 & 1 \\ 0 & 1 & 0 \\ -2K_f \frac{I_o}{M_s G_o^2} & 0 & 2K_f \frac{I_o^2}{M_s G_o^3} \end{bmatrix} \tag{8}$$

B. Disturbance Inputs

Stochastic Inputs: The stochastic inputs are random variations of the rail position during vehicle movement along the track. Considering the vertical direction, the velocity variations ($\dot{z}_t$) can be approximated by a double-sided power spectrum density (PSD) and the corresponding autocorrelation function, assuming a vehicle velocity, V_v of $15m/s$ and track roughness, $A_r = 1 \times 10^{-7}$ [11]. *Deterministic Input:* The main deterministic input to the suspension in the vertical direction is due to the transition onto the rail's gradients. In this work, the deterministic input corresponds to a rail gradient of 5% at a vehicle speed of $15m/s$, an acceleration of $0.5m/s^2$, and a jerk of $1m/s^3$ [11].

C. MAGLEV Control Requirements

The design requirements for an EMS system depend on the type and operating velocity of the train, discussed in [12]. The EMS system must support the payload while reject the stochastic inputs (from track roughness) and follow the deterministic ones (track gradients). Fundamentally, there is a trade-off between the deterministic and stochastic features, hence there are specific boundaries (see Table I) where they are allowed to operate.

TABLE I
Control Constraints for the MAGLEV Suspension.

Response requirements	Value
Stochastic track profile	
RMS of acceleration, $\ddot{z}_{rms}$	$\leq 0.5ms^{-2}$
RMS of airgap variation, $(z_t - z)_{rms}$	$\leq 5mm$
RMS of control effort, $u_{c_{rms}}$	$\leq 300V$
Deterministic track profile	
Maximum airgap deviation, $(z_t - z)_p$	$\leq 7.5mm$
Maximum control effort, u_{c_p}	$\leq 300V$
Settling time, t_s	$\leq 3s$
Airgap steady state error, $e_{(z_t - z)_{ss}}$	$= 0$
Zero input track profile	
RMS of the noise on control effort,$u_{n_{rms}}$	$\leq 50V_{rms}$

III. SENSOR OPTIMISATION FRAMEWORK VALIDATION USING FIL

A short description of the systematic framework is given in this section, whereas for the interested reader a rigorous description can be found in [1]. Moreover, the development of a systematic framework for optimised sensor selection for control via LQG is presented in [1], [10].

The problem is formulated as follows: Any industrial plant has a number of control inputs $\{u_i : i = 1, \dots n_u\}$, input disturbances $\{d_i : i = 1, \dots n_d\}$ and a set of possible outputs, i.e., the full sensor set, $\mathcal{Y}_f = \{y_i : i = 1, \dots n_s\}$. Part of the problem is to determine the set of sensors, $\mathcal{Y}_o \subset \mathcal{Y}_f$, for which the system is (i) stable, (ii) satisfies a number of closed-loop performance criteria and (iii) has a minimum number of sensing elements in the selected set, i.e., the number of elements in $\mathcal{Y}_o$ is minimal.

The selection of $\mathcal{Y}_o$ with respect to the aforementioned properties is a very important and complex process, especially if the plant has a large number of actuator/sensor configuration possibilities, i.e., sets. This work is focused upon optimised sensor selection, with respect to the aforementioned three properties. Figure 2 shows a typical control system diagram, which illustrates the optimised sensor selection problem for the control of the MAGLEV suspension system. The full sensor set $\mathcal{Y}_o$ shown in the figure is a subset of the full sensor set $\mathcal{Y}_f$. Many subsets of the full sensor set are possible to be formed, and the number of them can be calculated from $N_s = 2^{n_s} - 1$, where N_s is the total number of all sensor sets and n_s is the total number of sensors.

Given that the LQG controller is a combination of an LQR and a KBE, its tuning is done based on the separation principle as described in [2]; hence, the framework algorithm is executed in the next two steps:

(i) the LQR controller is optimised using a GA and the Pareto-optimality between the objective functions, i.e., $\phi_1 = i_{rms}$ and $\phi_2 = \ddot{z}_{rms}$ is found: In this step, the controller (i.e., state feedback gains, $K_{lqr} = [K_i \; K_{\dot{z}} \; K_{(z_t-z)} \; K_{\int(z_t-z)}]$), which results to the desired closed-loop response is selected and accounted as the 'ideal' or reference response for the second step, i.e., optimised tuning of the KBE.

(ii) The KBE is tuned for every feasible sensor set in order to achieve the 'ideal' closed-loop response. Eventually, a table is provided with the optimised sensor sets, where the "best" sensor set has been selected using the overall control constraint violation function Ω, given by,

$$\Omega(k^{(l)}, f^{(j)}) = \sum_{l=1}^{n_k} \omega_l(k^{(l)}) + \sum_{j=1}^{n_f} \psi_j(f^{(j)}) \qquad (9)$$

where $\omega_l(k^{(l)})$ and $\psi_j(f^{(j)})$ are the l^{th} and j^{th} soft and hard control constraint violations respectively, n_k and n_f are the number of soft and hard control constraints respectively, and Ω is a function where any control constraint violation is reflected. If all control constraints are satisfied Ω becomes zero, otherwise its value depends on the level of the constraints violation.

At the end, the selected sensor set was practically tested using FIL as it is depicted in Fig. 2. The latter figure clearly shows all five outputs, $\mathcal{Y}_f$ of a single degree of freedom MAGLEV suspension, out of which $\mathcal{Y}_o$ is fed into the FIL-based KBE. The MAGLEV along with the LQR are modelled in high-level using MATLAB/Simulink.

IV. FPGA Architecture of the Estimator

The linear time-invariant KBE has the following state space form,

$$\begin{aligned} \dot{\hat{x}} &= A\hat{x} + B_{u_c}u_c + K_{lqg}(y - C\hat{x}) && (10) \\ \hat{y} &= C\hat{x} && (11) \end{aligned}$$

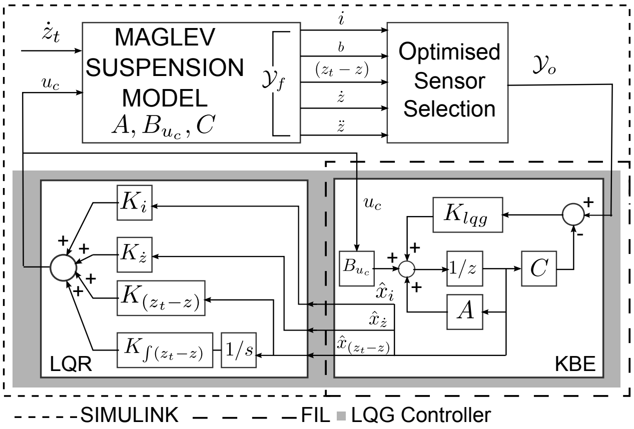

Fig. 2. Optimised sensor selection framework validation using FIL.

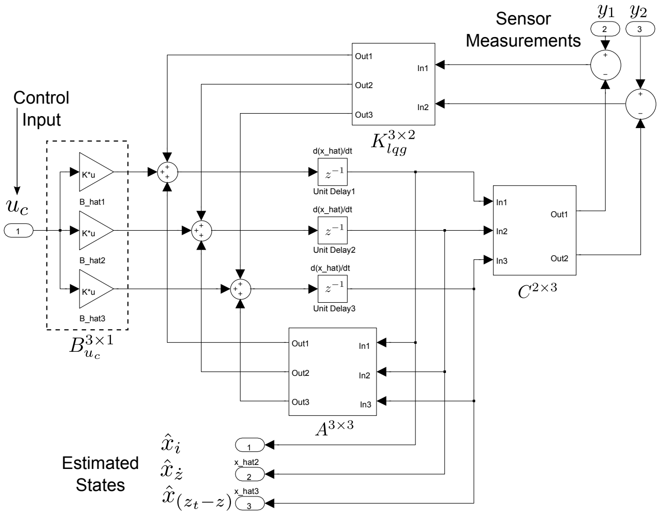

Fig. 3. KBE architecture for 2 sensor measurements (y_1, y_2).

where $\hat{x}$ are the estimated states and K_{lqg} is the $3 \times \beta$ observer gain matrix (β is the number of sensors) that minimizes $E\{[x-\hat{x}]^T[x-\hat{x}]\}$ (x represents the actual states). The design architecture of the KBE core implementation and its entity in Very High Speed Integrated Circuits (VHSIC) Hardware Description Language (VHDL) are depicted in Figs. 3 and 4 respectively. The internal architecture of $A^{3\times3}$ block is illustrated in Fig. 5, while a similar design approach is followed for $C^{\alpha\times3}$ and $K_{lqg}^{3\times\beta}$. The MATLAB HDL Coder tool was used in this work to automate and speed up the process of translating the high level simulation model to an equivalent Register Transfer Level (RTL) HDL (VHDL in our case). Due to MATLAB HDL Coder restrictions in handling multi dimension matrices, the KBE core (see Figs. 3 and 4) was implemented explicitly using scalar buses.

A. Quantization

An algorithm in a high level system modelling environment (such as MATLAB/Simulink) is represented in the floating-point domain, (mostly all variables are 64-bit) allowing all operations to be performed in high precision format with large accuracy. In a digital implementation this trans-

```
LIBRARY IEEE;
USE IEEE.std_logic_1164.ALL;
USE IEEE.numeric_std.ALL;

ENTITY Kalman_scalar_fxp IS
  PORT( clk                : IN  std_logic;
        rst                : IN  std_logic;
        clk_en             : IN  std_logic;
        control_i_p_u      : IN  std_logic_vector(31 DOWNTO 0);  -- sfix32_En25
        sensors_in_y1      : IN  std_logic_vector(31 DOWNTO 0);  -- sfix32_En28
        sensors_in_y2      : IN  std_logic_vector(31 DOWNTO 0);  -- sfix32_En36
        ce_out             : OUT std_logic;
        est_states_x_hat1 : OUT std_logic_vector(34 DOWNTO 0);  -- sfix35_En31
        est_states_x_hat2 : OUT std_logic_vector(34 DOWNTO 0);  -- sfix35_En33
        est_states_x_hat3 : OUT std_logic_vector(34 DOWNTO 0)); -- sfix35_En23
END Kalman_scalar_fxp;
```

Fig. 4. VHDL entity of the KBE core for 2 sensor measurements.

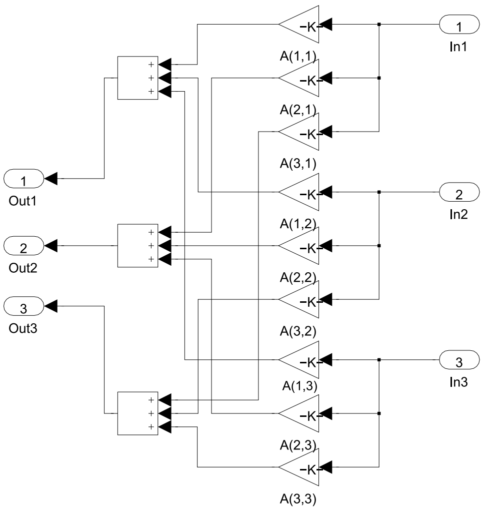

Fig. 5. $A^{3\times3}$ block internal architecture.

lates to an increased number of flip-flops and combinational logic and inevitably results on a design that requires a large silicon area on the chip, plus increased power consumption. To address the aforementioned problem, the algorithm under implementation (KBE in this work) must be first converted in the fixed-point domain and then described using VHDL. In the fixed-point domain, a pair of Wordlength, WL and Quality Fractional range, QF is considered for each parameter of the algorithm. As a consequence a larger (WL,QF) will give a smaller Bit-Error Rate (BER) but larger silicon area, and BER will increase (smaller silicon area) as (WL,QF) is reduced. Several simulations need to run to decide on the number of bits for (WL,QF) and the dynamic range of the parameters (MATLAB fixedpoint tool), in order to maintain a desired precision which will not compromise the overall system performance, and maintain a low silicon area.

The fixed-point range for a signed number $\pm a$ in a 2's complement form is defined by the minimum and maximum value range a signed integer number type of QI bits can hold. Hence,

$$-2^{QI-1} \leq a \leq 2^{QI-1} - 1, a \in \mathbb{Z} \tag{12}$$

or

$$-2^{QI-1} \leq a < 2^{QI-1} \tag{13}$$

where QI is the Quantity Integer range. From (13) it can be easily shown that, $QI|_{a_{min}} \geq \log_2(-a) + 1$ and $QI|_{a_{max}} > \log_2(a) + 1$.

Since the positive constraint is the tighter one due to the asymmetry of signed integer types about zero, the constraint for the required number of bits can be generalized as,

$$QI > \log_2(\max|[a_{min}, a_{max}]|) + 1 \tag{14}$$

From the above equation (since QI is an integer number of bits we can truncate the result and add one to form an equation to compute QI (that satisfies the constraint $QI > log_2(a)$) such as,

$$QI = \lfloor(\log_2(\max|[a_{min}, a_{max}]|) + 2\rfloor \tag{15}$$

for the fractional part assuming a resolution $\epsilon = 2^{-QF}$, the Quantity Fractional, QF range is,

$$QF = \lceil \log_2(\epsilon^{-1}) \rceil \tag{16}$$

Hence, the required wordlength, WL (to sufficiently represent a float number to a fixed point representation) is given by the sum of QI and QF, such that,

$$WL|_{Req} \geq QI + QF \tag{17}$$

or

$$-2^{QI-1} \leq a < 2^{QI-1} - 2^{-QF} \tag{18}$$

The inequality for the combined range and resolution is formally written as,

$$-2^{QI-1} \leq a \leq 2^{QI-1} - \epsilon \tag{19}$$

B. FPGA design and implementation

The FIL presented in this work was implemented on the Xilinx Spartan-6 SP605 development board. The SP605 board utilises a Xilinx Spartan-6 device (XC6SLX45T FGG484-3C) [13] in the 484-pin fine-pitch Ball Grid Array (BGA) package, featuring 6,822 slices [1]. The KBE and the peripheral cores were synthesized using Xilinx Synthesis Tool (XST). Table II shows the logic utilisation for the implemented integrated system on the FPGA device, which mainly includes the Kalman core, ethernet Medium Access Control (MAC) [14] and the Clock generator modules.

According to the device utilisation report from the Xilinx map (MAP) tool (see Table III), the KBE core itself occupies 74 slice registers, 790 slice LUTs, and 47 DSP cores (DSP48A1). The implemented design uses one Digital Clock Manager (DCM) module [15] that produces the different clocks inside the FPGA chip. The KBE design achieves a system clock operating frequency of 39.544ns or ∼25MHz. A top-level block diagram of the implemented KBE is shown in Fig.3 and Fig.5. The ethernet MAC core is licensed as part of the Xilinx Embedded Development Kit (EDK). The latter is a soft core, meaning that it is implemented using general logic primitives rather than a hard dedicated block into the FPGA. Its worth mentioning that the SP605 board features an ethernet physical interface transceiver (PHY) chip. The architecture of the present FIL consists mainly

[1] each slice contains 4 Look Up Tables (LUTs), 8 Flip-Flops (FFs) and special Digital Signal Processing (DSP) cores (DSP48A1)

of the KBE that communicates with the Simulink model through an ethernet link. The FPGA hosts the KBE filter, whereas the Simulink model mainly executes the MAGLEV system.

A top-down manner [16] has been followed for the design process of the KBE controller (see Fig.6). The process initiates with the model specifications and requirements, advances to a high level functional system model (Simulink model) and continues on converting it to fixed-point prior to FPGA implementation. Co-simulation of the RTL model side-by-side with the fixed-point Simulink model was performed using MATLAB's HDL verifier and Mentor's Modelsim simulator [17]. Moreover the implemented system on the FPGA chip was compared in real time using a cycle accurate Simulink model forming an FIL setup.

TABLE II

DESIGN RESOURCES.

Logic utilization	Used	Available	Utilization
Slice Registers	2,071	54,576	3%
Slice LUTs	3,636	27,288	13%
Fully used LUT-FF pairs	1,474	3,988	36%
Occupied Slices	1,287	6,822	18%
Bonded IOBs*	31	296	10%
Block RAMFIFO	5	116	4%
BUFG**	5	16	31%
DSP48A1s	47	58	81%
DCM/DCM_CLKGENs	1	8	12%

*IOBs: Input-Output Blocks, **BUFG: Global Clock Buffer

TABLE III

DESIGN RESOURCES PER MODULE WITH ONE SENSOR, b (ID:1).

	Total			
Module	**KBE**	**A**	**C**	K_{lqg}
Slices	51/274	80/80	29/29	114/114
Slice Registers	74/74	0/0	0/0	0/0
Slice LUTs	158/790	256/256	60/60	316/316
DSP48A1s	2/47	27/27	12/12	6/6

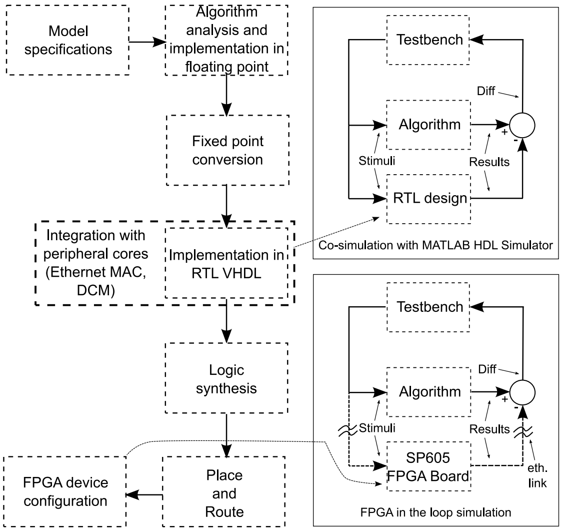
Model specifications
Algorithm analysis and implementation in floating point
Fixed point conversion
Integration with peripheral cores (Ethernet MAC, DCM)
Implementation in RTL VHDL
Logic synthesis
FPGA device configuration
Place and Route
Testbench
Diff
Algorithm
Stimuli
Results
RTL design
Co-simulation with MATLAB HDL Simulator
Testbench
Diff
Algorithm
Stimuli
Results
SP605 FPGA Board
eth. link
FPGA in the loop simulation

Fig. 6. HIL design and implementation flow.

V. RESULTS ANALYSIS

In this section, the results from the FIL combined with the systematic framework for optimised sensor selection are analysed. As explained in Section III, the first state vector K_{lqr} selection is based on three performance related criteria:

1) closed-loop vertical acceleration, $\ddot{z}_{rms} < 0.5m/s^2$,
2) excitation coil's current, $i_{rms} < 2A_{rms}$ and
3) best possible ride quality, i.e., $min(\ddot{z}_{rms})$.

The K_{lqr} gains are listed in Table IV. The second part of the framework is the optimisation of the KBE for each sensor set, where the aim here is to achieve the same closed-loop response for each sensor set as in the LQR design. The optimisation run has shown that 24 out of 31 sensor sets found to give the same closed-loop response as the LQR one. Some of the corresponding results from the offline framework are presented in Table V, where the first column is the sensor set identification number (id), the second column is the corresponding sensor set, and the next two columns show whether the stochastic and deterministic responses are satisfied (✓) or not (x). The last column is the overall constraint violation function, Ω, that similarly indicates if all control constraints listed in Table I are fulfilled (✓) or not (x). In this work the FIL is implemented only for three sensor sets, i.e., id:1, id:4 and id:7 and *only for the deterministic response* of the suspension, mainly due to the time consuming task of the KBE implementation flow on the FPGA. In future work, more sensor sets plus the stochastic response of the suspension will be addressed.

TABLE IV

LQR GAIN VECTOR, K_{lqr}, VALUES.

K_i	$K_{\dot{z}}$	$K_{(z_t-z)}$	$K_{\int (z_t-z)}$
V/A	V/(m/s)	V/m	V/m
-246.85	-3.366×10^3	2.145×10^5	2.417×10^5

TABLE V

OPTIMISED SENSOR CONFIGURATIONS VIA LQG CONTROL.

id	Sensor Set	Stochastic response	Deterministic response	Ω
	LQR response →	✓	✓	✓
1	b	✓	✓	✓
2	$(z_t - z)$	✓	x	x
3	$\ddot{z}$	✓	✓	✓
4	i, b	✓	✓	✓
5	$i, \ddot{z}$	✓	✓	✓
6	$i, b, (z_t - z)$	✓	✓	✓
7	$i, b, \ddot{z}$	✓	✓	✓
8	$i, b, \dot{z}, \ddot{z}$	✓	✓	✓
9	$i, b, (z_t - z), \dot{z}, \ddot{z}$	✓	✓	✓

The required performance of the suspension (using FIL with id:1, id:4 and id:7) under deterministic disturbance is fully met. Figures 7 and 8 depict the performance of the suspension (simulation-based and FIL with id:1). More specifically, Fig. 7 compares the airgap deflection from simulation-based continues-time and FIL-based discrete-time KBE. The airgap maximum deflection is less than $7.5mm$

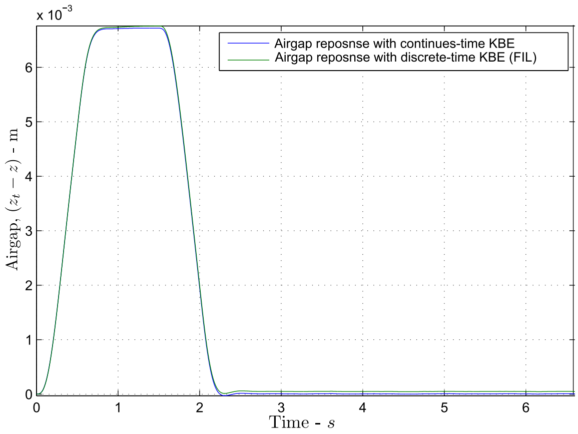

Fig. 7. Airgap results from simulation and FIL-based KBE with id:1.

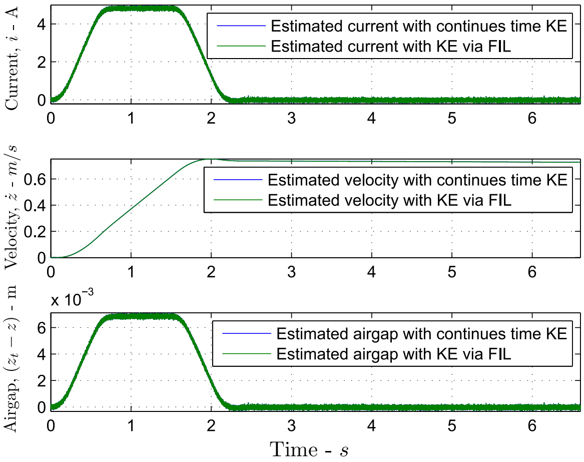

Fig. 8. State estimation from simulation and FIL-based KBE with id:1.

and returns to the operating point within less than $3s$, meaning that the response of the suspension fully complies with the control constraints on Table I. The state estimation of the KBE using the same sensor set (id:1) is shown in Fig. 8. All three states (i,$\dot{z}$ and $z_t - z$) are efficiently estimated using one measurement, which is similar to the state estimation if more sensors are added, e.g., id:4 and id:7.

VI. CONCLUSIONS

A semi-practical validation of the sensor optimisation framework was presented using the FIL concept. The MAGLEV suspension model is modelled in Matlab/Simulink environment and the KBE is implemented on an FPGA. A model-based design approach has been followed for the FIL implementation using a fusion of system modelling/verification and EDA tools. The effect of fixed-point quantization was analysed early in the design process and the wordlength was optimized to yield a smaller implementation. System level test benches were used with HDL co-simulation to verify the HDL implementation, and also FIL simulation to significantly accelerate the system validation. Three KBEs have been implemented in FIL for the deterministic response of the suspension, i.e., with sensor sets id:1, id:4 and id:7. The results clearly show that the KBE implementation in FIL is successful in spite of the non-trivial trial and error quantization procedure. Important properties such as reliability and robustness properties is an ongoing research and will be considered in future work.

REFERENCES

[1] K. Michail, A. Zolotas, and R. M. Goodall. Optimised configuration of sensors for fault tolerant control of an electromagnetic suspension system. *International Journal of Systems Science*, 43(10):1785–1804, 2012.

[2] S. Skogestad and I. Postlethwaite. *Multivariable Feedback Control Analysis and Design*. John Wiley & Sons Ltd, 2^{nd} Edition, New York, 2005.

[3] A. Konak, D.W. Coit, and A.E. Smith. Multi-objective optimization using genetic algorithms: A tutorial. *Reliability Engineering and System Safety*, 91(9):992–1007, 2006.

[4] Y. Zhang and J. Jiang. Bibliographical review on reconfigurable fault-tolerant control systems. *Annual Reviews in Control*, 32(2):229–252, 2008.

[5] M. Bacic. On hardware-in-the-loop simulation. In 44^{th} *IEEE Conference on Decision and Control and European Control Conference.*, pages 3194–3198, 2005.

[6] O. Lucia, O. Jimenez, L.A. Barragan, I. Urriza, J.M. Burdio, and D. Navarro. Real-time fpga-based hardware-in-the-loop development test-bench for multiple output power converters. In 25^{th} *Annual IEEE Applied Power Electronics Conference and Exposition (APEC)*, pages 309 –314, 2010.

[7] R. Isermann, J. Schaffnit, and S. Sinsel. Hardware-in-the-loop simulation for the design and testing of engine-control systems. *Control Engineering Practice*, 7(5):643–653, 1999.

[8] B. Lu, X. Wu, H. Figueroa, and A. Monti. A low-cost real-time hardware-in-the-loop testing approach of power electronics controls. *IEEE Transactions on Industrial Electronics*, 54(2):919–931, 2007.

[9] Xilinx Inc. Sp605 hardware user guide, UG526(v1.8), September 24, 2012. Available: www.xilinx.com/support/documentation/boards_and_kits/ug526.pdf.

[10] K. Michail, A. Zolotas, and R. M. Goodall. Optimised sensor configurations for a maglev suspension. *Proceedings of the* 17^{th} *World Congress The internetional Federation of Automatic Control*, pages 8305–8310, 2008.

[11] K. Michail. Optimised configuration of sensing elements for control and fault tolerance applied to an electro-magnetic suspension system, 2009. PhD dissertation, Loughborough University, School of Electronic, Electrical and Systems Engineering. http://hdl.handle.net/2134/5806.

[12] R. M. Goodall. Dynamics and control requirements for ems maglev suspensions. In *Proceedings on international conference on Maglev*, pages 926–934, 2004.

[13] Xilinx Inc. Spartan-6 family overview, DS160(v2.0) October 25, 2011. Available: www.xilinx.com/support/documentation/data_sheets/ds160.pdf.

[14] Xilinx Inc. Logicore ip tri-mode ethernet mac v4.5 user guide, UG138, March 1, 2011. Available: www.xilinx.com/support/documentation/ip_documentation/tri_mode_eth_mac_ug138.pdf.

[15] Xilinx Inc. Spartan-6 fpga clocking resources user guide, UG382(v1.7) July 20, 2012. Available: www.xilinx.com/support/documentation/user_guides/ug382.pdf.

[16] K. M. Deliparaschos, F. I. Nenedakis, and S. G. Tzafestas. Design and implementation of a fast digital fuzzy logic controller using FPGA technology. *Journal of Intelligent and Robotic Systems*, 45(1):77–96, January 2006.

[17] G.P. Moustris, K.M. Deliparaschos, and S.G. Tzafestas. Feedback equivalence and control of mobile robots through a scalabe FPGA architecture. In *Recent Advances in Mobile Robotics*. InTech, edited by: dr. andon venelinov topalov edition, 2011.